ALBERT-LUDWIGS-UNIVERSITÄT FREIBURG

MASTER THESIS

Readout of a five dimensional Calorimeter

Author:

Johannes ALT

Supervisor:

Prof. Dr. Horst FISCHER

February 8, 2023

Fakultät für Mathematik und Physik

Abstract

todo

Zusammenfassung

todo

Contents

Chapter 1

Introduction

So far the best physical description of the universe is provided be the Standard Model (SM). But through observations of different phenomena, which the SM can not explain, like neutrino oscillation [] and the rotation velocity in galaxies [], it is known, that the SM can not be a complete theory []. Therefore different experiments are in developement or are operating to search for new physics and new particles outside the SM. One of these experiments is the proposed Search for Hidden Particle (SHiP) experiment. Some experiments are at the energy frontier, using large energy scale trying to discover new particles. The experiments at the Large Hadron Colider (LHC) are examples for energy frontier experiments. Other experiments are at the cosmic frontieri, using for example cosmic background radiation. The third frontier is the intensity frontier. The zero background SHiP experiment is one of the intensity frontier experiment searching for rare events. Observing such rare events requires a high interaction rate. To achieve this, SHiP is planned to be a beam dump experiment at the Super Proton Synchrotron (SPS) accelerator ring at CERN, as shown in **??**. The goal is to dump the high intensity $400\,\mathrm{GeV}$ proton beam into a fixed target and thereby creating long lived particles outisde of the SM, e.g. heavy neutral leptons and light supersymmetric particles [1].

Figure 1.1: An overview of the SPS area with the SHiP experiment planed as beam dump experiment in the north area. [2]

Figure 1.2: Overview of the proposed setup for the SHiP experiment. The target on the left is used as a beam dump for the SPS. Most standard model particles get absorbed by the hadron absorber directly behind the targed. A magnetic muon shield deflects the muon, which won't be absorbed by the hadron absorber, away from the beam line. After the muon shield is a scattering and neutrino detector and afterwards the 50 m long decay volume in which non standard model particles created at the target can decay into standard model particles. To achieve the zero background goal, the Sourrund Background Tagger is around the decay volume. Behind the decay volume the decay spectrometer is placed. [3]

In **??** the overall struckture of SHiP is shown. At the beginning, the 400 GeV gets dumped into the fixed targed. Through the many interactions happening at the target, a lot of SM particles will be created. In order to block the SM particles, two shields are placed after the target. The first is a hadron absorber in which all SM particles except muons and neutrinos are absorbed. The second is the muon shield. It uses magnetic fields to deflect the muons away from the beam line. The neutrinos cannot be blocked or deflected, but they are likely to be detected in the scattering and neutrino detector behind the muon shield. After the neutrino detector a 50 m long vacuum chamber is positioned. If a non SM particle is created at the target, is can decay inside the vacuum decay chamber back into SM particles. The decay products than get measured in the decay spectrometer behind the decay chamber.

One problem for the measurement are SM particles entering the decay volume and causing events in the spectrometer. An example of such a background are muons deflected by the muon shield but afterwrads reflected by the walls of the facility into to decay volume. Therefore it is crucial for the zero background requirment to detect the particles entering the decay volume and tagging every event that could be caused by the entering particle as background. For this the Surround Background Tagger (SBT) is in developement. It is presented in the next chapter.

Chapter 2

One Cell Prototype

2.1   Silicon Photomultiplier

In order to correctly identify and tag background events, the light detection of the SBT has to provide accurate timing information. Therefore Silicon Photomultipliers (SiPMs) were chosen as photodetectors. These photodetectors consist of up to thousands of pixels. Each pixel is a photodiode with a typical edge length between $10\,\mu\text{m}$ and $100\,\mu\text{m}$ [5]. If triggered by light, a SiPM sends out a charge signal proportional to the incoming light. This charge possesses a fast-rising edge with a rise time of the order of tens of s [5]. Besides the good time resolution, SiPMs also make it possible to count the arriving photos with a sensitivity down to single photons [6].

Similar to every photodiode, Avalanche Photodiodes (APDs) utilize the photoelectric effect, to generate an electric charge signal in response to a light signal. This is made possible by using silicon as a base material and introducing impurities. This process is called doping and there are two different possibilities for doping. In the n-doping, the impurities are atoms with five valence electrons. Four of these electrons are part of boundings with silicon atoms, and the fifth electron is only weakly bound. When p-doping, atoms with only three valence electrons are inserted into the silicon. This leads to missing charges in the silicon, called holes. By having an n-doped and a p-doped region in the silicon, the excess electrons from the n-doped

Figure 2.1: Composition of a avalanche photo diode with the bias voltage V_B applied in reverse direction. Between the contact to ground and the strongly doped n^+ layer is the quenching resistor R_q connected in series. Next to the n^+ layer is a strongly doped p^+ layer. In the region of these two layers is the electric field, shown on the right figure, the strongest. There a electron or hole can initiate an avalanche. After the p^+ layer comes a intrinsic weakly doped π layer. This layer increases the sensitive volume of the diode. If a electron-hole pair is created and seperated by the electric field. The hole drifts towards the multiplication region and can start an avalanche. The next layer is a p^+ layer which connects to a metal connector and high voltage. [4]

region combine with the holes from the p-doped region, resulting in a depleted region at the pn-junction. If a photon hits the photodiode, it can create an electron-hole pair, or *eh*-pair. The electron and the hole get split by the electric field and thus create a charge signal. In order to increase the sensitivity of the photodiode, an intrinsic layer can be added in between the two doped regions, thus increasing the depletion layer and therefore the photosensitive area. Such a photodiode is called a pin-diode. An APD with a weakly doped π intrinsic layer and strongly doped p^+ and n^+ layers is shown in **??**. This intrinsic layer can either be not doped at all or weakly doped. In the case of APDs the intrinsic layer is weakly doped. In order to amplify the signal, a strong doped region is inserted, thus creating a multiplication zone.

When a reverse bias voltage is applied to the APD, the electric field between the n^+ and p^+ layers is strong enough that a created *eh*-pair creates more *eh*-pairs, resulting in an avalanche. For this avalanche process to be possible the reverse bias voltage must be at or above the breakdown voltage of the APD. With such a bias voltage applied, the APD operates in the Geiger mode and the avalanche is then self-sustaining. This results in a macroscopic signal and makes the detection of single photons possible. Therefore these diodes are also called Single Photon Avalanche Diode (SPAD). To stop the avalanche, a quenching resistor is connected in series with the SPAD. With an increasing current signal flowing through the quenching resistor, the voltage drop at this resistor increases, and thus the bias voltage at the SPAD decreases. When the bias voltage drops under the breakdown voltage, the avalanche is no longer self-sustaining and stops. Thus the signal amplitude of

a SPAD is always similar, independent of how many photons arrive at the same moment. In SiPMs hundreds to thousand SPADs are connected in parallel, each with a high resistance quenching resistor in series. Usually, the SPAD pixels are placed in a rectangular form with an edge length of a few mm. **??** shows a picture of a SiPM and one picture of a single pixel of a SiPM. Due to the property of the SPADs that the output signal is always similar for each SPAD, the output signal of a SiPM is the output signal of one SPAD multiplicated with the number of triggered SPADs. Therefore, if the number of photons arriving simultaneously at a SiPM is low enough, that the probability of one SPAD being hit by two or more photons is low, one can count photons with a SiPM. This and the relatively low cost, high durability, and impassivity to magnetic fields make them a good option for photodetection for the SBT and similar detectors.

In the following different properties of SiPMs are presented, beginning with the signal shape of a single SPAD and of a SiPM.

The signal shape of a SPADs starts with a fast exponential rise with the time constant

$$\tau_{\mathrm{rise}} = R_{\mathrm{S}} \cdot C_{\mathrm{d}} \tag{2.1}$$

with the resistance R_{rise} and capacitance C_{d} of the SPAD [6]. After the signal reached its maximum current at around

$$I_{\mathrm{max}} \approx \frac{V_{\mathrm{ov}}}{R_{\mathrm{q}}} \tag{2.2}$$

the quenching and recharging of the SPAD starts. Thus the current signal decreases again exponentially. The time constant for the signal decay

$$\tau_{\mathrm{decay}} = R_{\mathrm{q}} \cdot C_{\mathrm{d}} \tag{2.3}$$

depends on the capacitance C_{d} of the SPAD and the quenching resistor R_{q} [6]. This signal develpment is shown in **??**.

When multiple SPADs in a SiPM are triggered, the output signal will be the summation of the signals from all triggered SPADs. Besides the number of triggered

Figure 2.2: Single photon avalanche diode signal shape. The exponential rise with the time constant $R_{\mathrm{S}} \cdot C_{\mathrm{d}}$ is followed by the exponential decay with the time constants $R_{\mathrm{q}} \cdot C_{\mathrm{d}}$. The maximum of the current signal is at approximately $V_{\mathrm{ov}}/R_{\mathrm{q}}$ [6]

SPADs, the time difference between the signals from the single SPADs influences the signal. In the case, that all SPADs are triggered at the same time, the SiPM signal will have the shape of a SPAD signal scaled up by the factor of the number of triggered SPADs. If the signals form the individual SPADs have a small difference in time, the SiPM signal will become broader.

The gain G of a SiPM describes the number of charge carriers released in each avalanche. Due to the quenching, this parameter is well defined []. It can be calculated from the applied voltage U_{bias}, the breakdown voltage U_{bd} and the capacitance C_{d} of a SPAD with

$$G = \frac{(V_{\mathrm{bias}} - V_{\mathrm{bd}}) \cdot C_{\mathrm{d}}}{\mathrm{e}}. \tag{2.4}$$

Here e represents the charge of one electron. Usually the gain is in the order of 10^5 to 10^7 [5].

The noise   in SiPMs can be sorted into two categories. The first is primary noise, it describes the triggering of avalanches by thermaly created *eh*-pairs and not by incident photons. Because the rate of theses thermaly caused events increases and decreases with the temperature, by controling the temperatur one can influence and decrease the rate of primary noise events. The second category is the correlated noise. It includes all events triggered by a primary event. This correlated noise does have two causes. One cause is the trapping and releasing of charge carriers from the avalanche. When the time between the trapping and releasing is long enough, the avalanche of the primary event stoped and the released carrier can trigger another avalanche.

2.1.1   Photoelectron spectrum

After the theory and important properties of SiPMs are now introduced, the next chapter will present the measurement setup and data acquisition used for this thesis.

2.2   The eMUSIC Board

Since the signals of the SiPMs are very small, a single photolectron signal has an amplitude of around 2.5 mV, they need to be amplified. For this purpous the eMUSIC Application Specific Integrated Circuit (ASIC) by Scientifica was chosen and a custom Printed Circuit Board (PCB) housing the eMUSIC ASIC, from here on called eMUSIC board, was designed by the electrical engineers of the University of Freiburg. In the following first the ASIC itself and afterwards the eMUSIC board will be presented.

The eMUSIC ASIC   was developed by Scientifica for the readout of SiPMs. It is mainly an amplifier and a shaper, but also offers other options like digital trigger signals if the signal crosses an adjustable threshold. The ASICś block diagram is shown in **??**. It has eight input channels each equiped with a $\approx 1\,\text{V}$ anode voltage control to equalize the applied overvoltage between the different channels. Because the SiPMs deliver a charge signal, each channel has a current mode input stage. The eMUSIC ASIC was designed to have a low input transimpedance, but provides the option of a high transimpedance mode with which the gain can be increased. Each individual channel has bandwith of 150 MHz and a pole-zero cancellation, schematics shown in **??**, with two adjustable resistors and a adjustable capacitor. It can be used to decrease the **fwhm!** (**fwhm!**) of the output signal to below 10 ns.
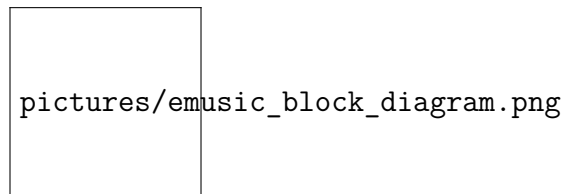

Figure 2.3: The block diagram of the eMUSIC ASIC.
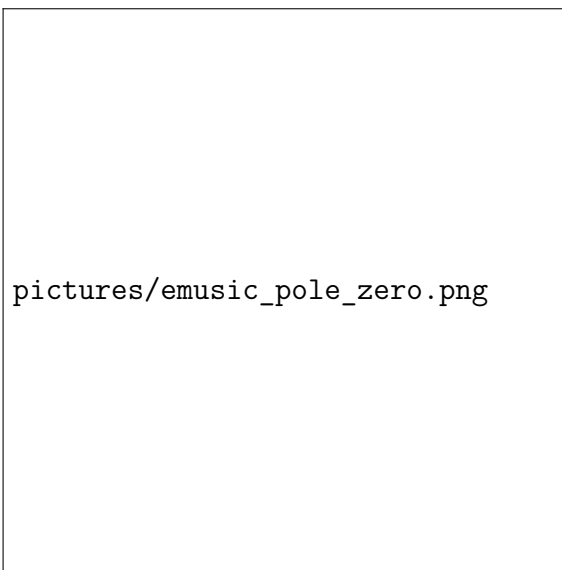
pictures/emusic_pole_zero.png

Figure 2.4: Sketch of a pole-zero cancellation with adjustable resistors and capacitor.

But a smaller width also attenuates the amplitude of the signal. The resistor has eight possible values it can be set to and the capacitor has thirty-two different steps. Although the eMUSIC provides the option of a lower attenuation mode of the pole-zero cancellation, a compromis between smaller signal width and higher amplitude should be chosen depending on ones needs. Alteratively the pole-zero cancellation can be disabled completely, resulting in the highest signal amplitude possible with the eMUSIC but also in the longest signal. The signal after the shaper can be put out with an analoge output for each channel.

Each channel also posseses a discriminator with an adjustable threshold to create a channel by channel trigger signal. These logical signals can be either put out by using the individual output of the channel for the digital signal instead for the analog waveform or by using the fast OR of all channels. This fast OR allows for example the external triggering of the digitzer which than digizes the analog waveforms if the waveform of one or more channels surpasses the threshold. The dynamic range of the output for the single edge signals is $1\,\mathrm{V}$ if the load on the output is $50\,\Omega$ and $2\,\mathrm{V}$ if a high impedance load is used on the ouput. Using the low transimpedance mode, the gain of the single edge output is $180\,\Omega$ and with the high transimpedance mode it is $480\,\Omega$. Over the first half of the dynamic range the response of the eMUSIC is linear and over the second half it is non-linear.

Besides the individual readout of the eight channels the eMUSIC can sum up the signal of an arbitrary set of channels with both high and low gain and put them out via two differential outputs. The bandwith of this summation output is 500 MHz and the output range is 1.25 V. Depending on wether the high or low transimpedance is used, the gain of the high gain summation is 690 Ω or 90 Ω and 315 Ω or 45 Ω for the low gain summation. The response of the summation output is linear over the dynamic range.

Besides choosing the channels for summation, also each of the eight single edge outputs can be individually turned on and off. Another important option that can be configered is the adjustment of the output DC offset to maximize the rail-to-rail voltage swing.

The trigger threshold for the digital outputs can be set with two parameters. The bandgap voltage V_{bg} of the comparators, which can be adjsuted in eight steps, to one of the following values:

$$V_{bg} = 487.22\,\text{mV}, 730.92\,\text{mV}, 974.62\,\text{mV}, 1218.3\,\text{mV}, 1462.0\,\text{mV}, 1705.7\,\text{mV}, 1949.4\,\text{mV} \, and \, 2436.8\,\text{mV}$$
$$(2.5)$$

The second parameter sets the Digital to Analog Converter (DAC) value N_{DAC} for the comparators. It can be set to DAC counts from 0 to 511. The finer threshold steps V_{fine} can be calculated with

$$V_{fine} = 1637.79\,\text{mV} - N_{DAC} \cdot 3.1445\,\text{mV}. \tag{2.6}$$

With V_{bg} and of V_{fine} or N_{DAC} the final threshold

$$V_{th} = 1.5 \cdot V_{bg} - 0.5 \cdot V_{fine} \tag{2.7}$$
$$= 1.5 \cdot V_{bg} - 0.5 \cdot (1637.79\,\text{mV} - N_{DAC} \cdot 3.1445\,\text{mV}) \tag{2.8}$$

can be calculated.

The eMUSIC board was designed at the University of Freiburg. A graphic of the board is shown in **??**. It's heart is the eMUSIC ASIC (U1). In order to program the ASIC the ATmega328P-AU microchip (U4) is placed on the board. The microchip

can be programed with the XXXX software by XXXXX and the XXXXX which is connected to the computer via USB and can be pluged into the J4 connector on the eMUSIC board. After programing the microchip it only has to be programed again if the reset button SW1 is pressed. Then the eMUSIC ASIC can be configered by using a TTL-to-USB adapter connected to a computer and the P3 connector and the software of the minimusic board. The minimusic board is a comercial product using the eMUSIC ASIC. Due to the eMUSIC board being designed to work with the minimusic software, one avoids the need to create a software and also has the security, that the used software was tested and is working properly. Two functions of the minimusic software are not usable on the eMUSIC board, the calibration of the threshold and the calibration of the DC offset on the outputs. Therefore theses two need to be set by the user.

The high voltage for the SiPMs can be supplied via the P2 SMA connector. On the backside of the PCB is a LSHM-150-XX.-XXX-DV-AN-XX connector located to connect the board to the SiPM board. Via this connector the high voltage is brought to the SiPMs and the signals are brought to the eMUSIC inputs. The eight single ended outputs can be read out by the SMA connectors K1 to K8. The fast OR signal can be read out via the K9 connector. Both the high and low gain differential summation outputs are connected to the pins of the J6 connector.

The board also provides the possibility via the P1 connector to power the six LEDs soldered onto the SiPM boards. But the usage of this is not advised, since this will introduce interferences into the signals.
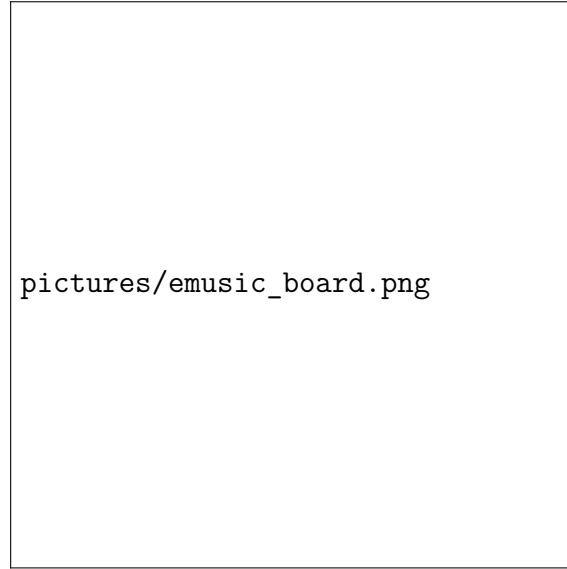
Figure 2.5: Picture of the eMUSIC board with the eMUSIC ASIC, the eight single ended channel by channel SMA signal outputs, the SMA fast OR output, the differential signal output, the SMA connector for the high voltage supply of the SiPMs and the connectors to program and power the board.

2.3 The Gandalf Framework

The amplified and shaped output signal of the eMUSIC ASIC needs to be digitized. This step is done by Gandalf modules. Originally developed at the University of Freiburg for the **compass!** (**compass!**) experiment it has a modular design to fill different roles in the experiments DAQ. Using mezzanin cards different signal, clock and trigger inputs can be chosen. In the following the Gandalf framework will be introduced. The mezzanin cards not used in this work are therefore only mentioned but not presented in detail. A overview of a Gandalf module is shown in **??**.

2.3.1 Input Mezzanin Cards

The Gandalf module has two mezzanin card slots for input signals. For these slots three different mezzanine cards were developed, **amc!** (**amc!**), **dmc!** (**dmc!**) and **omc!** (**omc!**). First the latter two mezzanine cards are shortly presented for completeness but are not relevant for the work done in this thesis.

Figure 2.6: Overview of the Gandalf module equiped with Analog Mezzanin Cards (AMCs) and the fiber Gimli mezzanin card for clock an trigger input. The analog waveforms are digitized by the AMCs and the digitized data is processed by the DSP FPGA. The MEM FPGA handles the memory of the processed data, which can be transfered to a computer via the USB inteface on the front of the VME or S-Link interfaces on the backplane. [**?**]

The dmc! has 64 digital inputs. A picture of it is shown in **??**. Using either the LVDS or the LVPECL signal standard, one can use the DSP-Field Programmable Gate Array (FPGA) logic for tasks like trigger decisions, time-to-digital conversion or pattern generators, to name a few. By changing the direction of the input buffer on the **dmc!** PCB, the 64 channels of the **dmc!** can be used as outputs intead of inputs.

The omc! has four 3.25 Gs transceivers to receive digital informations, which can be further processed by the DSP-FPGA. With this mezzanine card, the GANDALF can be used for example to merge data or as a concentrator. A picture of a **omc!** is shown in **??**.

The amc! is designed to digitize analog input signals. For the digitization, eight Analog to Digital Converter (ADC) are used. There are **amc!** with two different ADC available. One is the *ADS5463* with 12 and up to $500\,\frac{\text{MS}}{\text{s}}$ and the other is the *ADS5474* which samples with up to $400\,\frac{\text{MS}}{\text{s}}$ at 14. The **enob!** (**enob!**) of both ADCs are 10.4 and 11.2 respectively. Each **amc!** has eight SMC connectors for the inputs. There are **amc!** operating in *normal mode*, meaning each SMC connector is connected to one ADC, resulting in eight channels with up to $500\,\frac{\text{MS}}{\text{s}}$ or $400\,\frac{\text{MS}}{\text{s}}$ per **amc!**. In order to increase the sample frequency, **amc!** which operate in the *interleaved mode* were build. On these **amc!**s four inputs are connected to two ADCs each and therefore every second SMC connector is a dead end. The clock signals which provide the sample tact for the two ADCs of one channel have 180° phase offset in respect to each other. By this the sample frequency is doubled to up to $1\,\frac{\text{GS}}{\text{s}}$ or $800\,\frac{\text{MS}}{\text{s}}$, but the number of channels per **amc!** is reduced from eight to four. The dynamic input range of the **amc!** is 4.4 and can be shifted from the negative unipolar range $-4.4\,\text{V}$ to $0\,\text{V}$ up to the bipolar range $-2.2\,\text{V}$ to $2.2\,\text{V}$. This shifting is done by a *AD5665R*, a 16 DAC. The dynamic range was chosen because in the COMPASS experiment, for which the GANDALF was developed, negative voltage pulses created by Photomultiplier tubes (PMTs) needed to be digitized. But because the used ADCs expect positive differential signals, inverting operational amplifiers are used to change the polariy of the signal. By changing the gain of the amplifiers one can decrease the input range and therefore increase the amplitude resolution.

The **amc!**s used in this thesis are 12 **amc!**s in the *interleaved mode* and a dynamic range of 2.2.

2.3.2   GIMLI Mezzanine Cards

The third mezzanine card slot is for the GIMLI mezzanine cards, which are responsible for the clock and external trigger signals. For this mezzanine card, three different options were developed. One GIMLI card, which takes the clock and trigger from the backplane, if one wants to use the create to distribute the signals. The fiber GIMLI, which has one fiber input to reseive the clock and trigger via optical fiber. And the copper GIMLI, which was used for this work and is presented in the following.

The copper GIMLI   , shown in **??**, provids the option to use an external or an internal clock. If only one GANDALF module is used the internal 20 MHz clock of the copper GIMLI can be used. It is provieded by a on board oven controlled oscillator (OCXO) with a jitter less than 2.3 ps. In case two or more GANDALFs are used an external clock is required to ensure a synchronized clock on all GANDALF modules. For this case, the copper GIMLI has a LEMO connector as input for an external clock with **nim!** (**nim!**) signal standard. Via a second LEMO connector an external **nim!** trigger signal can be connected to the GANDALF module.

2.3.3   Usage of the GANDALF with SiPMs

In this work, the GANDALF was used to digitize the ouput signal of the eMUSIC **asci!** (**asci!**). As mentioned in above in **??** theses signals have a positive polarity. But because the GANDALF was designed for the digitization and processing of negative voltage pulses created by a PMT, this caused some problems. Since after the inverting operational amplifiers in the GANDALF the SiPM signals have a negative polarity, the input voltage range needs to be chosen to be bipolar and around -1.1 V to 1.1 V. In order to get this input range the baseline at 0 V would need to be set to 2047 ADCu. For unknown reasons the programm which configeres the DACs to set the baseline to a ADCu value selectable by the user will set the baseline
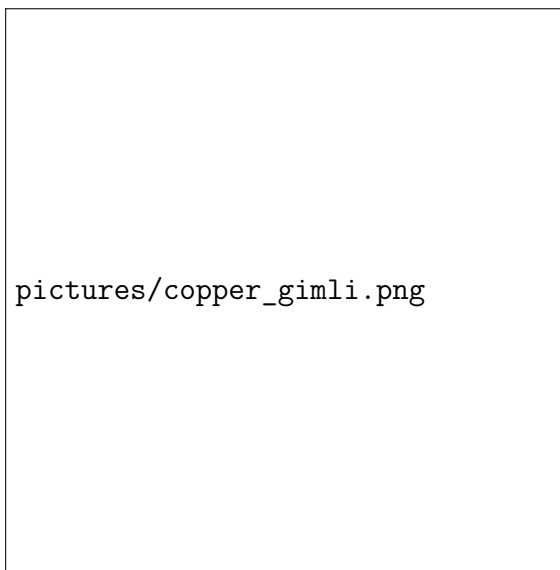
Figure 2.7: Picture of the copper GIMLI with an internal 20 MHz clock generated by an on board oven controlled oscillator. With the LEMO connectors external clock and trigger **nim!** signals can be provided for the GANDALF.

to a maximum of around 1400 ADCu. With $\frac{2.2}{2^{12}} \frac{\text{V}}{\text{ADCu}} = 0.537 \frac{\text{mV}}{\text{ADCu}}$ the range of the inverted signal is 1400 ADCu which corresponds to approximately 752 mV. Should this range be not enough, one needs to either try to find the source of the problem and fix it or decrease the amplification of the eMUSIC ASIC.

The next problem regards the self-trigger of the GANDALF. It functions via samples-over-threshold, the user can set a threshold and a number of consecutive samples which need to be over the threshold for the GANDALF to trigger an event. Since after the inverting of the positive signals the signals have a negative polarity, the threshold needs to be set to a lower ADCu value than the baseline. In addition to that the sample-over-threshold condition in the GANDALF firmware needed to be inverted to trigger if a number of consecutive samples are below the threshold. The new firemware with the inverted trigger condition was tested and works as intended with the exception of one bug. If the data rate from the GANDALF to the DAQ computer exceeds the maximum possible data rate, 20 Ms in case of the USB inteface, incomplete events will be written down to disk. This is most likely caused by a missing VHDL file that was not included in the new firmware and which would, incase the buffer of the GANDALF is completly filled, prevent the GANDALF to

send incomplete events to the computer. For the intended use of this bug should not be a problem, since the data rate is expected to be way below the possible 20 Ms.

Chapter 3

Setup

Chapter 4

Results of the DAQ tests

4.1 Input offset voltage

4.2 Pole-zero cancellation

4.3 High and low transimpedance and lower attenuation

4.4 Dark count measurements

Chapter 5

DAQ performance at the DESY testbeam

After the performance of the DAQ was tested at the testbeam for one week with particles of known energy and known direction of movement, the long term performance of the one cell prototype and the DAQ needs to be investigated. For this purpose, the one cell prototype is assembled at the University of Freiburg, where it is supposed to be taking continuously data for a year.

Chapter 6

Summary and Outlook

Appendix A

List of acronyms

SM   Standard Model

LHC   Large Hadron Colider

SHiP Search for Hidden Particle

SPS   Super Proton Synchrotron

SBT   Surround Background Tagger

SiPM Silicon Photomultiplier

PCB   Printed Circuit Board

ASIC Application Specific Integrated Circuit

DAC   Digital to Analog Converter

ADC   Analog to Digital Converter

APD   Avalanche Photodiode

DAQ   Data Acquisition

WOM   Wavelengthshifting Optical Module

SPAD Single Photon Avalanche Diode

DC   Dark Count

DCR Dark Count Rate

FPGA Field Programmable Gate Array

DESY Deutsches Electronen SYnchrotron

eMUSIC enhanced Multiple Use SiPM IC for photodetector readout

PMT Photomultiplier tube

List of Figures

List of Tables

Bibliography

[1] SHiP - Search for Hidden Particles, `https://ship.web.cern.ch/`, June 2022

[2] S. Alekhin et al "A facility to search for hidden particles at the CERN SPS: the SHiP physics case", Rep. Prog. Phys. 79, Oct 2016, `https://doi.org/10.1088/0034-4885/79/12/124201`

[3] SHiP Collaboration, "SPS Beam Dump Facility - Comprehensive Design Study", 2020, arXiv:1912.06356

[4] J. Kemp, "Development of a silicon photomultiplier based scintillator detector for cosmic air showers" Phd thesis, Dez 2020, RWTH Aachen

[5] F. Acerbi, S. Gundacker, "Understanding and simulating SiPMs", NIM-A vol. 926, p. 16-35, 2019. doi: 10.1016/j.nima.2018.11.118

[6] Hamamatsu Photonics, MPPC, `https://www.hamamatsu.com/content/dam/hamamatsu-photonics/sites/documents/99_SALES_LIBRARY/ssd/mppc_kapd9005e.pdf`, date: 20.06.2022

[7] Hamamatsu S14160-3050HS Datasheet, `https://www.hamamatsu.com/content/dam/hamamatsu-photonics/sites/documents/99_SALES_LIBRARY/ssd/s14160_s14161_series_kapd1064e.pdf`, date: 05.05.2022

[8] Weeroc Citiroc 1A Datasheet V2.5, `https://www.weeroc.com/my-weeroc/download-center/citiroc-1a/16-citiroc1a-datasheet-v2-5/file`, date: 09.05.2022

[9] J. Grieshaber, "Calculation and simulation of Silicon photomultiplier signals", B.Sc. thesis, Feb 2022, ALU Freiburg